expression constitutes an evolutionally conserved mechanism for governing time-dependent stem cell fates, including temporal fate progression in neural stem cells and their derived neuronal lineages.

REFERENCES AND NOTES

1. P. Mattar, J. Ericson, S. Blackshaw, M. Cayouette, *Neuron* **85**, 497–504 (2015).
2. P. Gao *et al.*, *Cell* **159**, 775–788 (2014).
3. X. Li, Z. Chen, C. Desplan, *Curr. Top. Dev. Biol.* **105**, 69–96 (2013).
4. M. Kohwi, C. Q. Doe, *Nat. Rev. Neurosci.* **14**, 823–838 (2013).
5. J. W. Truman, W. Moats, J. Altman, E. C. Marin, D. W. Williams, *Development* **137**, 53–61 (2010).
6. S. Lin *et al.*, *Development* **137**, 43–51 (2010).
7. T. Lee, A. Lee, L. Luo, *Development* **126**, 4065–4076 (1999).
8. S. Lin, C. F. Kao, H. H. Yu, Y. Huang, T. Lee, *PLOS Biol.* **10**, e1001425 (2012).
9. H. H. Yu *et al.*, *PLOS Biol.* **8**, e1000461 (2010).
10. X. Li *et al.*, *Nature* **498**, 456–462 (2013).
11. T. Isshiki, B. Pearson, S. Holbrook, C. Q. Doe, *Cell* **106**, 511–521 (2001).
12. T. Awasaki *et al.*, *Nat. Neurosci.* **17**, 631–637 (2014).
13. K. J. Venken, J. H. Simpson, H. J. Bellen, *Neuron* **72**, 202–230 (2011).
14. S. M. McDermott, C. Meignin, J. Rappsilber, I. Davis, *Biol. Open* **1**, 488–497 (2012).
15. T. P. Munro, S. Kwon, B. J. Schnapp, D. St Johnston, *J. Cell Biol.* **172**, 577–588 (2006).
16. C. Geng, P. M. Macdonald, *Mol. Cell. Biol.* **26**, 9508–9516 (2006).
17. J. R. Crittenden, E. M. Skoulakis, K. A. Han, D. Kalderon, R. L. Davis, *Learn. Mem.* **5**, 38–51 (1998).
18. T. Awasaki *et al.*, *Neuron* **26**, 119–131 (2000).
19. X. Zheng *et al.*, *Cell* **112**, 303–315 (2003).
20. S. Zhu *et al.*, *Cell* **127**, 409–422 (2006).
21. C. Medioni, M. Ramialison, A. Ephrussi, F. Besse, *Curr. Biol.* **24**, 793–800 (2014).
22. P. Lasko, *RNA* **2**, 408–416 (2011).
23. Y. V. Svitkin *et al.*, *PLOS Biol.* **11**, e1001564 (2013).
24. H. Toledano, C. D'Alterio, B. Czech, E. Levine, D. L. Jones, *Nature* **485**, 605–610 (2012).
25. J. Nishino, S. Kim, Y. Zhu, H. Zhu, S. J. Morrison, *eLife* **2**, e00924 (2013).

ACKNOWLEDGMENTS

We thank L. Jones, T. S. Hays, P. Macdonald, and I. Davis for sharing reagents. We thank the Transgenic RNAi Project at Harvard Medical School (NIH/NIGMS R01-GM084947) and the Vienna Drosophila Resource Center for providing transgenic RNAi fly stocks used in this study. We thank R. Miyares, G. Rubin, J. Truman, C. Wu, and I. Davis and his group for comments. This work was supported by Howard Hughes Medical Institute. RNA-sequencing data are available in the National Center for Biotechnology Information Gene Expression Omnibus, accession no. GSE71103. The supplementary materials contain additional data.

SUPPLEMENTARY MATERIALS

www.sciencemag.org/content/350/6258/317/suppl/DC1
Materials and Methods
Figs. S1 to S8
Table S1
References (*26*–*29*)

5 August 2015; accepted 16 September 2015
10.1126/science.aad1886

OCEAN VARIABILITY

The Atlantic Multidecadal Oscillation without a role for ocean circulation

Amy Clement,[1]* Katinka Bellomo,[1] Lisa N. Murphy,[1] Mark A. Cane,[2] Thorsten Mauritsen,[3] Gaby Rädel,[3] Bjorn Stevens[3]

The Atlantic Multidecadal Oscillation (AMO) is a major mode of climate variability with important societal impacts. Most previous explanations identify the driver of the AMO as the ocean circulation, specifically the Atlantic Meridional Overturning Circulation (AMOC). Here we show that the main features of the observed AMO are reproduced in models where the ocean heat transport is prescribed and thus cannot be the driver. Allowing the ocean circulation to interact with the atmosphere does not significantly alter the characteristics of the AMO in the current generation of climate models. These results suggest that the AMO is the response to stochastic forcing from the mid-latitude atmospheric circulation, with thermal coupling playing a role in the tropics. In this view, the AMOC and other ocean circulation changes would be largely a response to, not a cause of, the AMO.

The observed variability of North Atlantic sea surface temperatures (SSTs) is characterized by a horseshoe pattern (Fig. 1A) and a predominately multidecadal time scale (Fig. 1C). This pattern is commonly referred to as the Atlantic Multidecadal Oscillation (AMO). The AMO index is defined as the average SST from 0° to 60°N, 80°W to 0°, detrended to isolate the natural variability (*1*). Temperature changes associated with the AMO have been shown to affect weather and climate around the North Atlantic basin and possibly throughout the global tropics (*1*–*6*). However, the physical mechanism of the AMO is not well understood.

[1]Rosenstiel School of Marine and Atmospheric Science, University of Miami, Miami, FL, USA. [2]Lamont-Doherty Earth Observatory of Columbia University, New York, NY, USA. [3]Max Planck Institute for Meteorology, Hamburg, Germany.
*Corresponding author. E-mail: aclement@rsmas.miami.edu

Previous explanations for the AMO have focused almost exclusively on the role of naturally occurring changes in ocean circulation, primarily the Atlantic Meridional Overturning Circulation (AMOC) (*7*–*12*). Based on model experiments and paleoclimate proxy data, it has been suggested that at times when the AMOC is weak, or at the extreme, completely shut down, the North Atlantic ocean cools because of reduced northward ocean heat transport (*9*, *13*). Direct observational evidence that this mechanism explains 20th-century AMO variability is not available, because continuous measurements of the AMOC have only been available since 2004. In climate models, the AMOC and North Atlantic SST are correlated (weak AMOC when the North Atlantic is warm), but there is no robust lead-lag relationship between the two (*11*, *14*), which makes it difficult to argue that AMOC changes drive SST changes in models. In addition to the AMOC, some studies have made a case for a strong aerosol forcing of this variability (*15*, *16*), but this has been disputed in recent studies (*17*, *18*).

Although the causes of the AMO are unclear, climate models are nonetheless capable of reproducing the spatial pattern of observed SST variability and the associated changes in atmospheric circulation. Figure 1B shows the pattern of SST, sea-level pressure (SLP), and surface winds regressed on the AMO index derived from a subset of fully coupled climate models that participated in the Coupled Model Intercomparison Projects 3 and 5 (CMIP3/5) (Table 1 and methods). In these simulations, the climate forcings (greenhouse gases, anthropogenic aerosols, orbital parameters, and solar irradiance) are prescribed at preindustrial values, so simulated variability arises from "natural" processes internal to the climate system. Earlier studies have attempted to show that these simulated natural variations in North Atlantic SST are the surface expression of the internal variability in the ocean circulation, the AMOC in particular (*11*, *14*, *19*, *20*).

Here we show, however, that this pattern of variability can be produced without ocean circulation changes. To do so, we used results from the same atmospheric general circulation models used in Fig. 1B, coupled to a 50-m-deep slab-ocean mixed-layer model (hereafter referred to as slab-ocean models), rather than being coupled to an ocean general circulation model (hereafter referred to as fully coupled models). Slab-ocean simulations are run with constant preindustrial forcing and a prescribed annual cycle of ocean heat transport (methods). In these models, the atmosphere and ocean exchange heat and moisture (hence are thermally coupled), but because the ocean heat transport is unchanging, it cannot drive SST variability. Despite the absence of interactive ocean circulation, the slab-ocean models are capable of widespread warming of the North Atlantic. The spatial pattern and magnitude (Fig. 1D) of the slab-ocean simulations are indistinguishable from those of their coupled model versions

(Fig. 1B), with a pattern correlation of 0.87 (Table 2). Furthermore, the magnitude of the AMO index variance is similar in the multimodel mean of fully coupled (0.053) and slab-ocean (0.058) models (Table 1), which compares with the 0.051 mean of the three observational data sets. (methods). These results are unchanged if we isolate only low-frequency variability in the AMO index (fig. S1).

Whereas conventional wisdom is that interactive ocean circulation is important in generating decadal to multidecadal time scale climate variability, the spectral characteristics of the slab-ocean and fully coupled models are nearly indistinguishable. Figure 2A shows that the spectra of the multimodel mean preindustrial slab-ocean simulations are essentially the same as those of the fully coupled models. For periods longer than 10 years (beyond the El Niño/Southern Oscillation band of 2 to 7 years), both resemble a red noise process, suggesting that there is nothing distinctive about decadal and multidecadal variability in these models. The same is true of the later-generation CMIP5 models (Fig. 2B). It may be objected that individual fully coupled models have low frequency spectral peaks that are averaged out in the ensemble mean. However, Fig. 3, which shows the spectra of the North Atlantic SST index for individual models, makes it clear that this is not the case (Fig. 3 includes all the fully coupled models that have a respective slab-ocean simulation of at least 70 years in length; Table 1). The only fully coupled model that produces variability at decadal or longer time scales that is significantly greater than in the slab-ocean version is the GFDL_CM2_1 model. The enhanced quasidecadal variability in the fully coupled version of this model is mainly in the sub-polar gyre (fig. S2) which suggests that it is tied to the ocean circulation, but it is not clear whether it is enhanced by the AMOC or by the upper ocean sub-polar gyre circulation. Three of the fully coupled

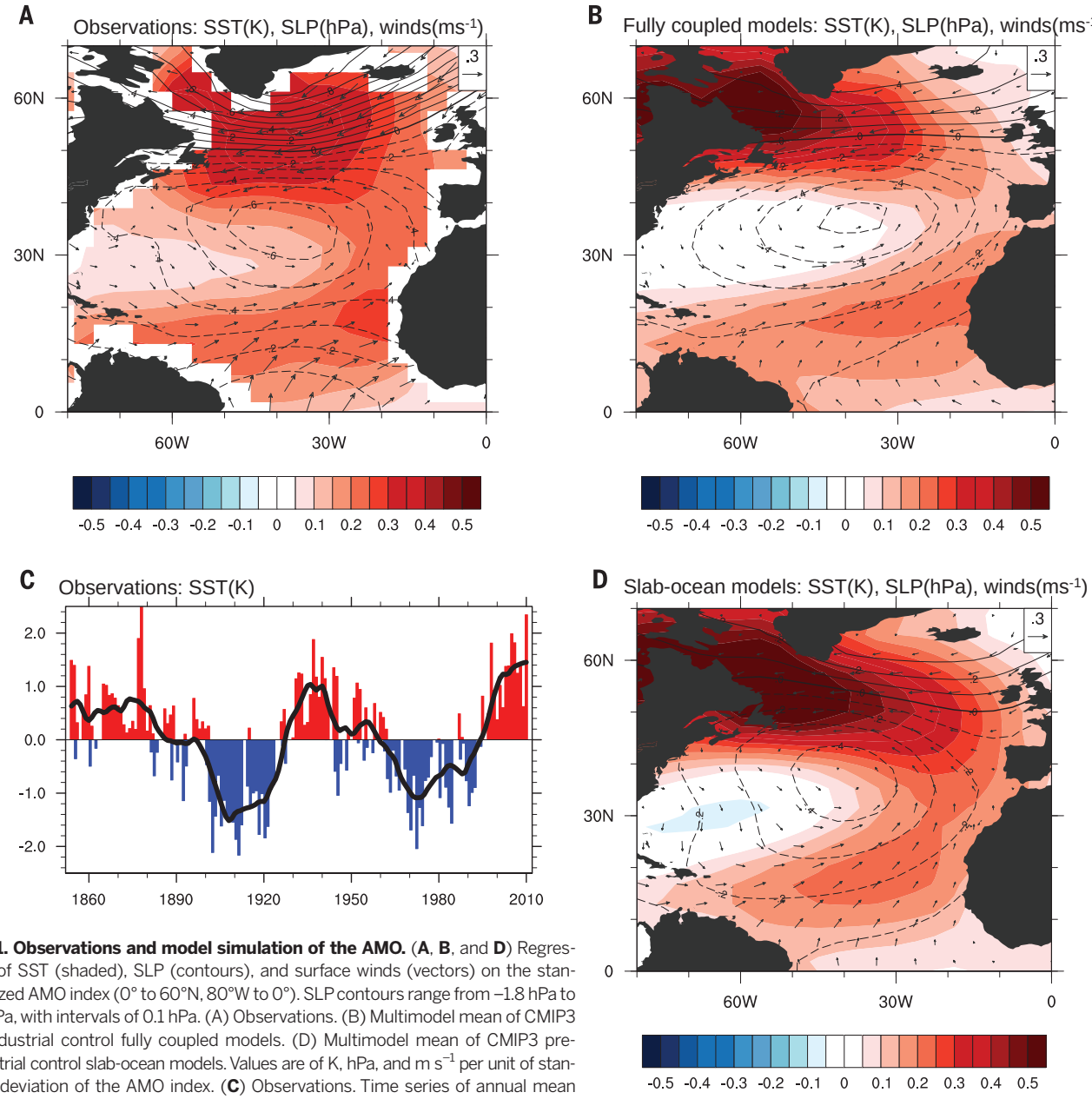

Fig. 1. Observations and model simulation of the AMO. (**A**, **B**, and **D**) Regression of SST (shaded), SLP (contours), and surface winds (vectors) on the standardized AMO index (0° to 60°N, 80°W to 0°). SLP contours range from –1.8 hPa to 1.8 hPa, with intervals of 0.1 hPa. (A) Observations. (B) Multimodel mean of CMIP3 preindustrial control fully coupled models. (D) Multimodel mean of CMIP3 preindustrial control slab-ocean models. Values are of K, hPa, and m s^{-1} per unit of standard deviation of the AMO index. (**C**) Observations. Time series of annual mean anomalies of the standardized AMO index (colored bars) with a 10-year running average superimposed (black line). The observed SST is from ERSSTv3b, whereas surface winds and SLP are from the NCEP/NCAR (National Centers for Environmental Prediction/National Center for Atmospheric Research) reanalysis. All fields are detrended.

models produce peaks at shorter interannual time scales that are not present in the slab-ocean model (Fig. 3), but this is due to the tropical Atlantic response to El Niño/Southern Oscillation, which is known to influence the tropical Atlantic (*21*).

Our interpretation of these results is that the AMO is the response of the upper ocean mixed layer to forcing by the atmosphere, projecting mostly on the North Atlantic Oscillation (NAO), with thermal coupling playing a fundamental role in generating the tropical component of the AMO signal. The NAO is a mode of atmospheric variability, which represents a shift in the westerly jet in the Atlantic basin, along with a change in strength of the subtropical high. The wind and SLP patterns associated with the AMO (Fig. 1A) clearly show the NAO signature: Periods when the North Atlantic is warm occur when the subtropical high is weak and the westerly jet shifts poleward, resulting in weaker westerly winds in the mid-latitudes. The NAO itself is internal to the atmosphere and does not require coupling with the ocean (*22*, *23*). This is demonstrated in Fig. 4A, which shows the NAO in the Community Atmosphere Model version 4 (CAM4) forced with climatological SST (CAM4-sstClim). This pattern has no dependence on time scale, and the power spectra of the mid-latitude surface winds are consistent with white noise (fig. S3) as in previous studies (*24*).

However, observations, slab-ocean models, and fully coupled models simulate surface wind changes in the tropics associated with the AMO, which can explain the tropical part of the horseshoe warming pattern (*25*) (Fig. 1, A, B, and D). These wind changes are absent in the uncoupled CAM4-sstClim model (Fig. 4A), and only when the atmosphere is coupled to the slab-ocean model do the tropical winds show a response to the NAO (Fig. 4B). The spectra of the tropical meridional winds in the slab-ocean model are slightly red, with considerably enhanced variability (fig. S3), which we interpret as arising from thermal coupling between the atmospheric circulation and the mixed-layer ocean, and adding year-to-year persistence to otherwise uncorrelated variability.

Coherent changes in SST and trade winds in the northern tropical Atlantic due to thermal coupling have been extensively documented and arise from a wind-evaporation–SST feedback (*26*, *27*). Weaker winds in the northern tropics induce weaker evaporation, resulting in warmer SST. The SST change then drives a low-level wind response, which allows the signals to expand equatorward. It has also been suggested that a local positive feedback between atmospheric circulation, SST, and low-level clouds can contribute to the persistence of these climate anomalies (*28*). Thus, thermal coupling between the mixed-layer ocean and the atmosphere in the northern tropics results in a warming of the North Atlantic Ocean that extends into the tropics as the low-frequency response to the NAO.

The pattern of the AMO in these unforced simulations is not perfectly correlated with the observed pattern (Table 2). The most likely cause of the difference is model biases in their simulation of the mean climate. Because their resolution is coarse (~1° to 2°), all of these models underestimate the strong SST fronts in the Gulf Stream region, which leads to differences in the patterns and magnitude of variability in that region. It is possible that high-resolution global climate models, which are starting to become available, may simulate more of a role for the ocean circulation than do current-generation models. There are also persistent biases in the simulation of the tropical Atlantic climate in coupled models, which can imprint on the

Table 1. Variance of the AMO index (0° to 60°N, 80°W to 0°) in observations, preindustrial slab-ocean model simulations, and their respective fully coupled model versions. All time series are detrended. Observational values cover the years 1920–2014.

Data set	Length of slab-ocean models (years)	Length of fully coupled models (years)	Resolution (latitude × longitude)	AMO variance	
Kaplan			5.0° × 5.0°	0.046	
ERSSTv3b			2.0° × 2.0°	0.056	
HADISST			1.0° × 1.0°	0.052	
				AMO variance in slab-ocean models	*AMO variance in fully coupled models*
Multi-Model Mean				0.058	0.053
CCCMA_CGCM3_1	30	500	3.75° × 3.75°	0.052	0.068
CCCMA_CGCM3_1_T63	30	350	2.8° × 2.8°	0.069	0.054
GFDL_CM2_0	50	500	2.0° × 2.5°	0.053	0.064
GFDL_CM2_1	100	500	2.0° × 2.5°	0.054	0.063
INMCM3	60	330	4.0° × 5.0°	0.084	0.049
MIROC3_2_HIRES	20	500	1.125° × 1.125°	0.052	0.041
MIROC3_2_MEDRES	60	100	2.8° × 2.8°	0.055	0.044
MPI_ESM_LR	180	1000	3.75° × 3.75°	0.047	0.056
MRI_CGCM2_3_2A	100	350	2.8° × 2.8°	0.038	0.043
NCAR_CCSM4	450	500	0.90° × 1.25°	0.049	0.042
UKMO_HADGEM1	70	240	1.25° × 1.75°	0.115	0.078
GISS_MODEL_E_R	120	500	3.9° × 5.0°	0.031	0.037

Table 2. Spatial correlations between regressions of SST on the standardized AMO index in various observational and multimodel mean data sets. All data are detrended.

	Kaplan	ERSSTv3b	HadISST	Slab-ocean models	Fully coupled models	PiCntrl (CMIP5)	Historical (CMIP5 1865 to 2005)
Kaplan	1						
ERSSTv3b	0.84	1					
HadISST	0.90	0.88	1				
Slab-ocean models	0.79	0.83	0.77	1			
Fully coupled models	0.76	0.70	0.68	0.87	1		
PiCntrl (CMIP5)	0.80	0.70	0.68	0.85	0.96	1	
Historical (CMIP5 1865–2005)	0.76	0.62	0.60	0.74	0.90	0.97	1

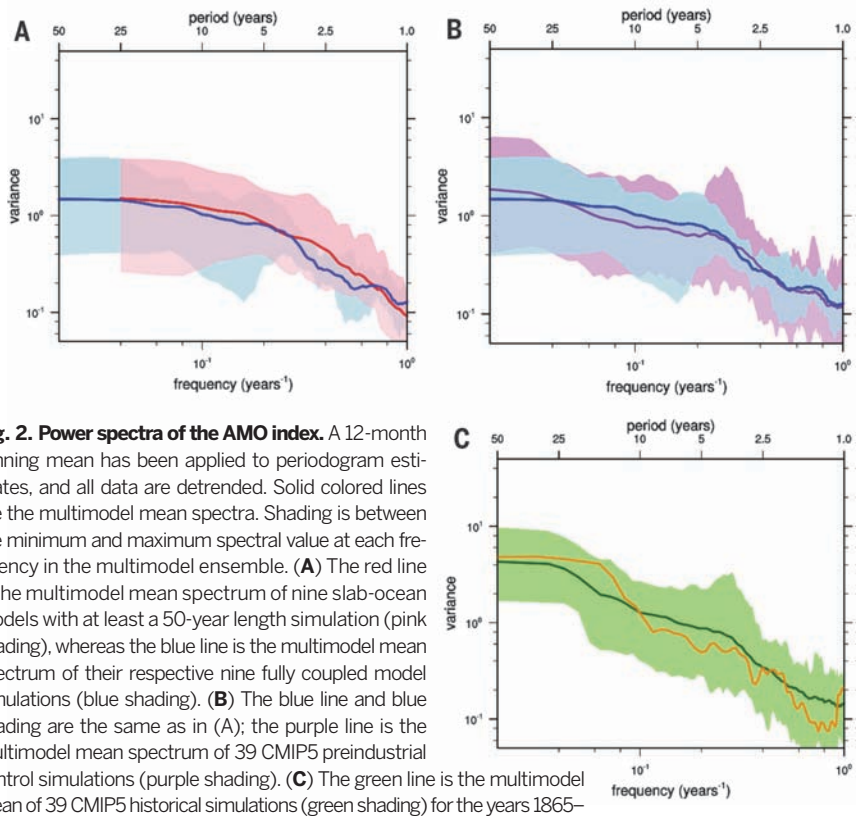

Fig. 2. Power spectra of the AMO index. A 12-month running mean has been applied to periodogram estimates, and all data are detrended. Solid colored lines are the multimodel mean spectra. Shading is between the minimum and maximum spectral value at each frequency in the multimodel ensemble. (**A**) The red line is the multimodel mean spectrum of nine slab-ocean models with at least a 50-year length simulation (pink shading), whereas the blue line is the multimodel mean spectrum of their respective nine fully coupled model simulations (blue shading). (**B**) The blue line and blue shading are the same as in (A); the purple line is the multimodel mean spectrum of 39 CMIP5 preindustrial control simulations (purple shading). (**C**) The green line is the multimodel mean of 39 CMIP5 historical simulations (green shading) for the years 1865–2005. The orange line is the power spectrum of the observed AMO index from ERSSTv3b for the years 1920–2014.

pattern of variability. The fact that the slab-ocean models have a higher correlation with the observed pattern is likely due to the fact that those models have a SST climatology prescribed from observations, whereas coupled-model climatologies exhibits significant SST biases, a problem that perhaps worsens in CMIP5 as compared to CMIP3, as evident in the correlations in Table 2. The inclusion of historical climate forcings in model simulations does not improve the pattern correlation with observations (Table 2).

It could be argued that the preindustrial simulations underestimate the magnitude of observed multidecadal variability (Fig. 2C). The inclusion of historical climate forcings does enhance multidecadal variability, bringing it into better agreement with observations (Fig. 2C), although it has been shown that several models overestimate the impact of atmospheric aerosols (*18*). On the other hand, a possible source of persistence that is missing in climate models is cloud feedbacks, particularly in the tropical Atlantic (*28*). Climate models show a strong sensitivity of low-level marine cloudiness to thermodynamic variations of the mean state (*29*), whereas observations show that cloudiness covaries much more strongly with low-level winds, and in ways that would amplify the interactions discussed here (*30*). Proper simulation of these feedbacks may lead to models with enhanced low-frequency variability in the Atlantic basin (*31*).

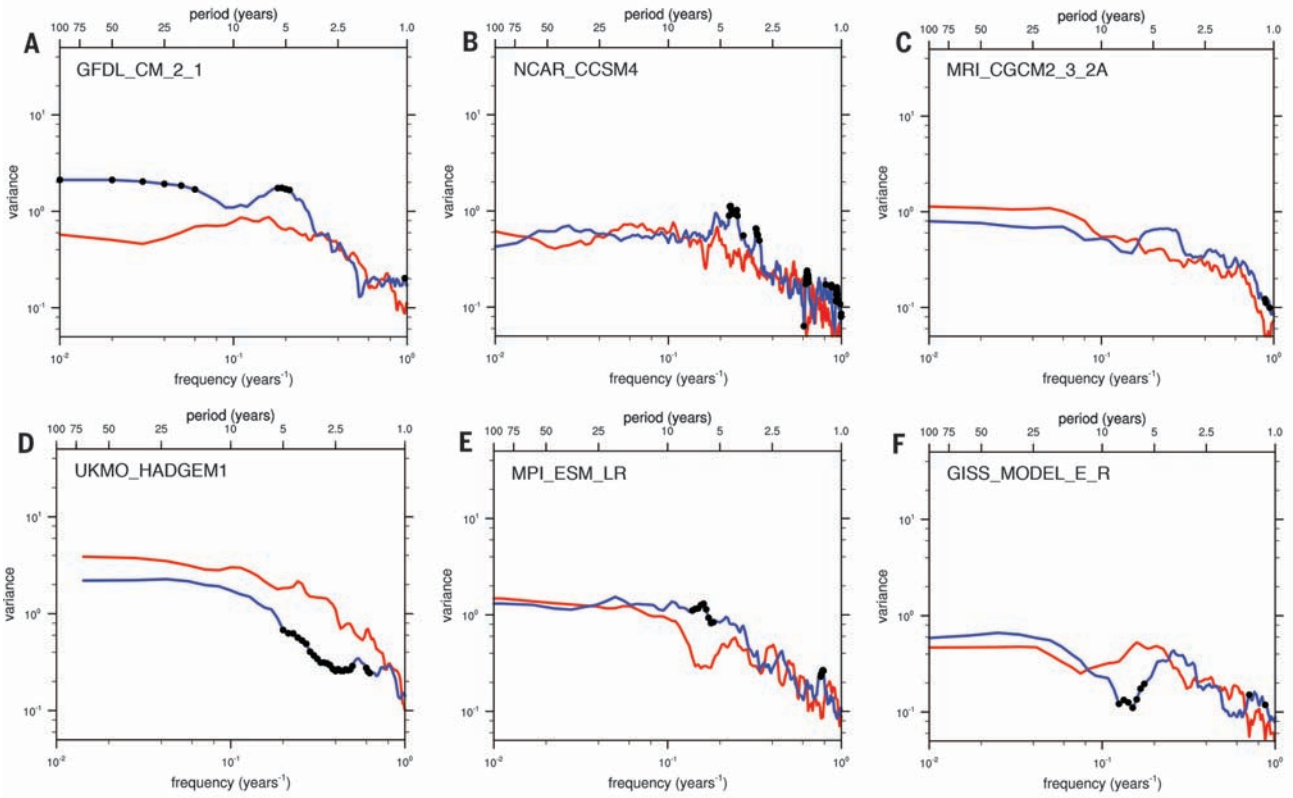

Fig. 3. Paired power spectra of the AMO index in models with at least 70 years of simulation (Table 1). Red curves are for the slab-ocean simulations; blue curves are for their respective coupled simulations. A 12-month smoothing has been applied to the periodogram estimates, and all data are detrended. Black markings indicate where the variance of the blue curve is significantly different than the variance of the red curve at the 95% confidence level according to Fisher's *F* test.

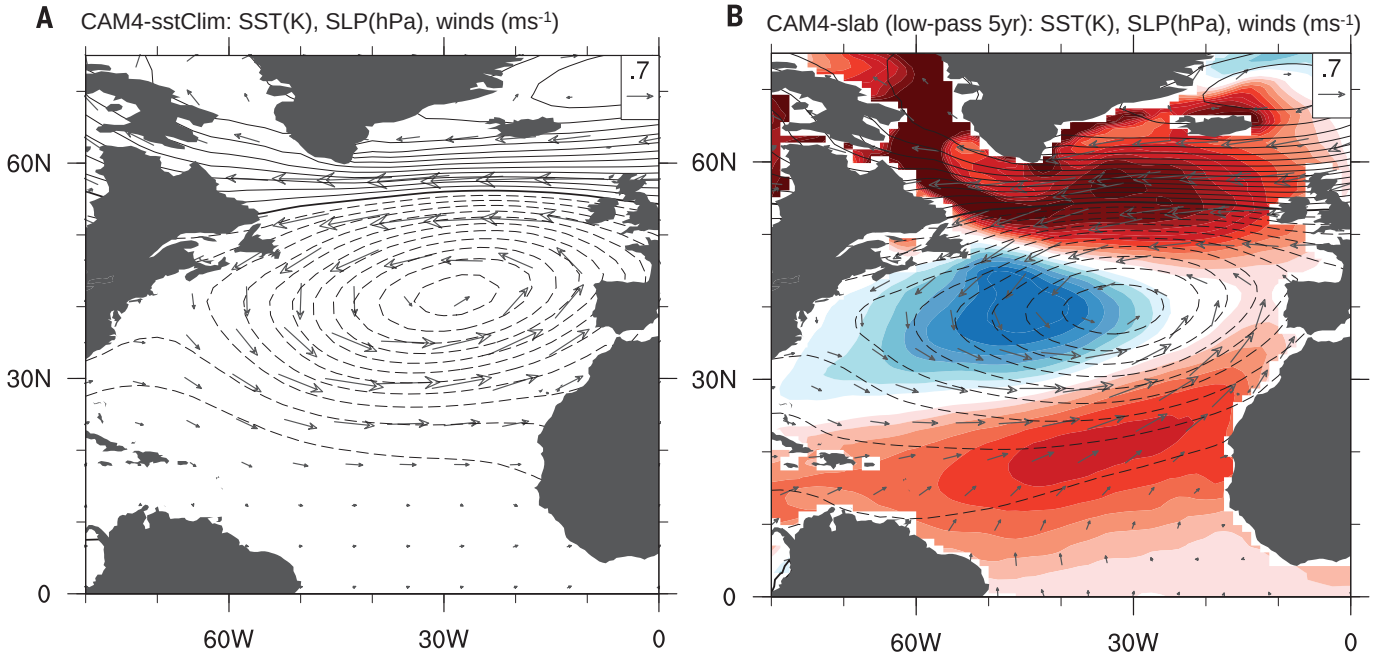

Fig. 4. The NAO in an uncoupled and a slab-ocean model. Regression of SST (shaded), SLP (contours), and surface winds (vectors) on the standardized Subtropical High (SH) index (the SLP averaged over 25° to 40°N to 45°W to 20°W) for (**A**) the CAM4-sstClim simulation, in which the SSTs are fixed and set to climatology and (**B**) the CAM4-slab simulation that includes thermal coupling. In (B), the SH index is filtered using a low-pass Lanczos filter to remove variability in the sub–5- year time scale. Units are of °C, hPa, and m s^{-1} per standard deviation of the SH index. SLP contours range from −4 hPa to 4 hPa, with intervals of 0.25 hPa.

We have shown that simulations of the AMO using fully coupled atmosphere-ocean models, which produce spatial and temporal characteristics consistent with observations, are essentially indistinguishable from those produced by the equivalent slab-ocean model versions, which lack interactive ocean dynamics. Instead, the simplest explanation for the AMO is that it is the low-frequency response to the high-frequency atmospheric "noise" embodied, for example, in the NAO, with thermal coupling extending the signal into the tropics to produce the characteristic horseshoe pattern of warming. The ocean circulation, including surface layer Ekman currents and possibly the AMOC (*32*, *33*), would respond to these changes in atmospheric circulation as demonstrated by McCarthy *et al.* (*34*), but a feedback from the ocean circulation on the AMO is not supported by our analysis. Our analysis does not rule out that the ocean circulation may contribute to low-frequency variability in parts of the ocean, such as the subpolar gyre, as suggested in (*34*). Nor does it rule out the possibility that massive changes in the AMOC suggested in the paleoclimate record had profound consequences for global climate (*13*). However, the current-generation models analyzed here do not support the idea that ocean circulation drives the AMO.

REFERENCES AND NOTES

1. D. B. Enfield, A. M. Mestas-Nunez, P. J. Trimble, *Geophys. Res. Lett.* **28**, 2077–2080 (2001).
2. R. T. Sutton, D. L. R. Hodson, *Science* **309**, 115–118 (2005).
3. J. R. Knight, C. K. Folland, A. A. Scaife, *Geophys. Res. Lett.* **33**, L17706 (2006).
4. V. A. Semenov *et al.*, *J. Clim.* **23**, 5668–5677 (2010).
5. R. Zhang, T. L. Delworth, *Geophys. Res. Lett.* **33**, L17712 (2006).
6. R. A. Kerr, *Science* **309**, 41–43 (2005).
7. T. Delworth, S. Manabe, R. J. Stouffer, *J. Clim.* **6**, 1993–2011 (1993).
8. M. Latif *et al.*, *J. Clim.* **17**, 1605–1614 (2004).
9. T. L. Delworth, M. E. Mann, *Clim. Dyn.* **16**, 661–676 (2000).
10. J. R. Knight, R. J. Allan, C. K. Folland, M. Vellinga, M. E. Mann, *Geophys. Res. Lett.* **32**, L20708 (2005).
11. C. Z. Wang, L. P. Zhang, *J. Clim.* **26**, 6137–6162 (2013).
12. J. Ba *et al.*, *Clim. Dyn.* **43**, 2333–2348 (2014).
13. R. Zhang, T. L. Delworth, *J. Clim.* **18**, 1853–1860 (2005).
14. N. F. Tandon, P. J. Kushnir, *J. Clim.* **28**, 6309–6323 (2015).
15. M. E. Mann, K. A. Emanuel, *Eos* **87**, 233, 238, 241 (2006).
16. B. B. Booth, N. J. Dunstone, P. R. Halloran, T. Andrews, N. Bellouin, *Nature* **484**, 228–232 (2012).
17. R. Zhang *et al.*, *J. Atmos. Sci.* **70**, 1135–1144 (2013).
18. B. Stevens, Rethinking the lower bound on aerosol radiative forcing. *J. Clim.* (2015), http://journals.ametsoc.org/doi/abs/10.1175/JCLI-D-14-00656.1.
19. M. Klöwer, M. Latif, H. Ding, R. J. Greatbatch, W. Park, *Earth Planet. Sci. Lett.* **406**, 1–6 (2014).
20. C. Marini, C. Frankignoul, *Clim. Dyn.* **43**, 607–625 (2014).
21. D. B. Enfield, D. A. Mayer, *J. Geophys. Res.* **102**, 929–945 (1997).
22. I. M. Held, in *Large-Scale Dynamical Processes in the Atmosphere*, B. J. Hoskins, R. F. Pearce, Eds. (Academic Press, New York, 1983), pp. 127–169.
23. R. Saravanan, *J. Clim.* **11**, 1386–1404 (1998).
24. C. Wunsch, *Bull. Am. Meteorol. Soc.* **80**, 245–255 (1999).
25. R. Seager *et al.*, *J. Clim.* **13**, 2845–2862 (2000).
26. S. P. Xie, *J. Clim.* **12**, 64–70 (1999).
27. J. C. H. Chiang, D. J. Vimont, *J. Clim.* **17**, 4143–4158 (2004).
28. A. T. Evan, R. J. Allen, R. Bennartz, D. J. Vimont, *J. Clim.* **26**, 3619–3630 (2013).
29. X. Qu, A. Hall, S. A. Klein, P. M. Caldwell, *Clim. Dyn.* **42**, 2603–2626 (2014).
30. M. Brueck, L. Nuijens, B. Stevens, *J. Atmos. Sci.* **72**, 1428–1446 (2015).
31. K. Bellomo, A. Clement, T. Mauritsen, G. Rädel, B. Stevens, *J. Clim.* **28**, 2725–2744 (2015).
32. T. L. Delworth, R. J. Greatbatch, *J. Clim.* **13**, 1481–1495 (2000).
33. M. Visbeck, H. Cullen, G. Krahmann, N. H. Naik, *Geophys. Res. Lett.* **25**, 4521–4524 (1998).
34. G. D. McCarthy, I. D. Haigh, J. J. Hirschi, J. P. Grist, D. A. Smeed, *Nature* **521**, 508–510 (2015).

ACKNOWLEDGMENTS

This work was supported by grants from the U.S. Department of Energy and the National Oceanographic and Atmospheric Administration. M.A.C. was supported by Office of Naval Research grant N00014-12-1-0911. The authors are grateful to Y. Kushnir, G. Schmidt, B. Kirtman, C. Frankignoul, and C. Deser for lively discussions. All CMIP data are available at http://cmip-pcmdi.llnl.gov/. Data from simulations with the CAM4 model can be obtained by e-mailing the corresponding author.

SUPPLEMENTARY MATERIALS

www.sciencemag.org/content/350/6258/[page]/suppl/DC1
Materials and Methods
Figs. S1 to S3
References (*35*–*41*)

21 April 2015; accepted 18 September 2015
10.1126/science.aab3980